SPE-177628-MS

# New Insights on the Mechanical Characterization of Kerogen-Rich Shale, KRS

Katherine L. Hull, Aramco Research Center--Houston; Younane N. Abousleiman, University of Oklahoma; Yanhui Han, Aramco Research Center--Houston; Ghaithan A. Al-Muntasheri, Saudi Aramco; Peter Hosemann, S. Scott Parker, and Cameron B. Howard, UC-Berkeley



This paper was prepared for presentation at the Abu Dhabi International Petroleum Exhibition and Conference held in Abu Dhabi, UAE, 9–12 November 2015.



## Abstract

In the past decade, chemical, physical and mechanical characterization of source rock reservoirs has moved towards micro- and nano-scale analyses, primarily driven by the fact that the representative elementary volume (REV) for characterizing shales is at the nanometer scale. Nanoindentation is now widely used in many industrial and university laboratories to measure both stiffness and strength mechanical properties of shales, such as anisotropic Young's Moduli and plastic yielding parameters. However, to date, tensile failures of shales have not been studied at the micro- or nanoscale.

In this work, a nanoindenter is used to bring organic-rich shale (preserved Woodford shale from a well site in Ada, Oklahoma) to failure in tension. Micro-cantilever beam geometries (~25 microns in length and ~5 microns in width) were milled and loaded to failure while monitoring *in-situ* via scanning electron microscopy (SEM). The force-displacement curves were analyzed in light of the high resolution images collected during fracture initiation, propagation, and ultimate failure. Complementary studies of the mineralogical composition, particularly at the failure faces, as well as the organic content were also performed. Failure planes and tensile fracture initiation in the micro-beam were associated with the various phases of the mineral and organic cluster components.

The micro-beam tests of this composite natural material demonstrate linear elastic behavior followed by plastic yielding before complete failure. This behavior was clearly observed to correlate with the amount of organic matter at the fractured surface. Energy dispersive X-ray spectroscopy (EDS) analyses were conducted at the post-failure stage on the resulting fracture faces and the relationship between mechanical behavior and composition was established. It was observed that when high mineral content was found at the faces, a brittle failure took place, while when the fixed support had high kerogen content the micro-beam failed in a ductile mode.

These results reinforce our growing understanding of the heterogeneous nature of shale and the importance of nano- and micro-scale analyses to understand our reservoir source rocks.

## Introduction

Recent technological advances in the oil and gas industry have led to economical production in unconventional source rock reservoirs such as shales. These rocks are fine-grained with natural fractures and nanoporous matrices composed of nano-granular clay and microscale non-clay minerals (Ma et al. 2014, Chalmers et al. 2012). Kerogen, the hydrocarbon source material, is also interbedded with the minerals and is an organic polymer-like material which can characteristically vary depending on its type and maturity (Passey et al. 2010). Figure 1(a) and (b) demonstrate the nature of interlacing that occurs between the rock matrix (light gray) and organic matter (dark gray). The organic matter can have a globular structure or more string-like configuration as shown in these images. Overall, these kerogen-rich shales (KRS) are highly complex natural materials that are difficult to characterize chemically, physically, and mechanically.

The structural complexity of shales occurs on all scales (macro-, micro-, and nanometer), highlighting the need for characterization methods that probe the material at the finest scales. Structurally, the nanoscale data includes chemical analysis of both the shale minerals and their arrangement, composition of the organic matter (e.g., kerogen or bitumen) (Schuler et al. 2015; Feng et al. 2013), as well as the pore and fracture structures and their interfaces. Focused ion beam

(FIB) milling and electron microscopy have been widely used to prepare and image, respectively, very small shale samples in order to develop a detailed understanding of their structures (Curtis et al. 2010). Mechanical characterization has also been achieved at the nanoscale using methods such as nanoindentation to determine Young's modulus and hardness of both the rock matrix and the elastomeric kerogen (Zeszotarski et al. 2004, Ulm and Abousleiman 2006). These early attempts to micro-mechanically characterize gas shale (Woodford) at the nano- and micro-scales through load-displacement measurements demonstrated the intrinsic stiffness micro-anisotropy of these fine-grained heterogeneous rocks. Figure 1(c) provides a typical load-unload displacement curve, collected during indentation into gas shale, which is used to determine the shale elastic moduli (Oliver and Pharr 1992).

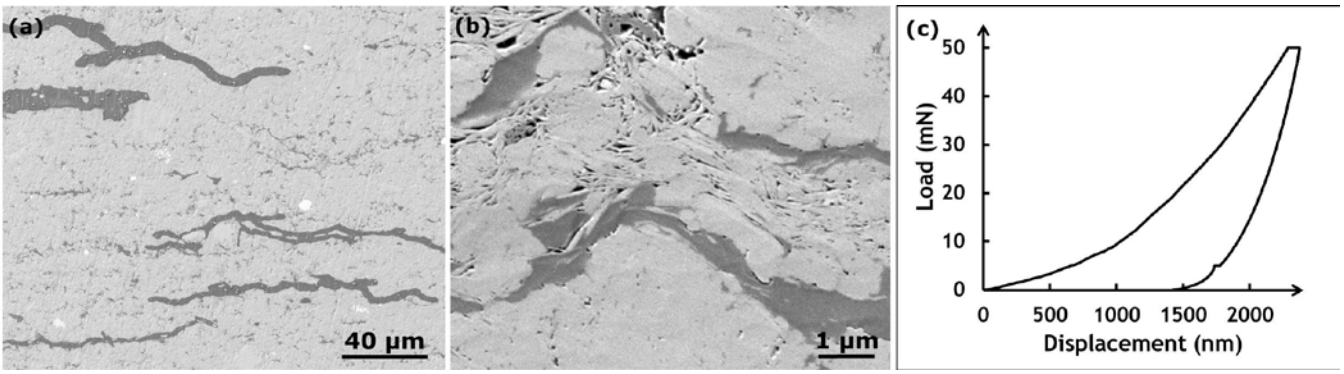


**Figure 1.** Woodford shale (a) is depicted in the SEM image taken with the microscope oriented parallel to bedding. (b) A second SEM image is shown in the same orientation but at a much smaller scale. Indentation performed on this type of material gave rise to the load-displacement curve shown in (c).

These methods have concentrated on the micro- and nanoscale characterization of the elastic response of shale, and the hardness of its phases. Recently, the plastic yield parameters and deformation using the nanoindenter were also explored, adding substantive value to the growing body of knowledge of KRS (Bennett et al. 2015). The nanoindenter has now been expanded as a method to measure the tensile strength of KRS, by loading and failing micro-cantilever geometries (Abousleiman et al. 2015). Existing ISRM methods for determining the tensile strength of KRS such as the Brazilian test cannot sufficiently identify the micro effects of the interlacing kerogen into the overall clay and non-clay matrices. The method introducted here is broadly used in various material science laboratories for analyzing failure mechanisms and fracture toughness of various manmade materials (Hosemann et al. 2008, 2013).

Here we demonstrate that this method provides a sophisticated tool for measuring the tensile strength of KRS in that it accounts for contributions from both the rock and the organic matter. Micro-beams are manufactured with a focused ion beam under a scanning electron microscope (FIB-SEM) with dimensions of ~25 microns in length and <10 microns in their prismatic section. The beams are then loaded in cantilever mode with a nanoindenter, where a fracture forms near the support then propagates and ultimately leads to beam tensile failure. The kerogen which is intertwined within the rock matrix is shown to drastically increase the tensile strength of the rock, even as much as 100 times more than any tensile strength of shale ever measured before. An implication of this finding is that a significant amount of energy at the pumps will be needed to propagate fractures in these reservoirs.

## Methods

Two small samples (<1 cm in all three dimensions) were cut from a preserved Woodford shale core. The first sample was milled with a Retsch Mixer Mill MM400 to obtain a powder. The powder was analyzed via x-ray diffraction (XRD) with a Bruker D8 Advance Eco powder diffractometer then analyzed using Rietveld refinement to determine the mineral constituents. A portion of the sample was also tested by a Shimadzu SSM-5000 total organic carbon (TOC) analyzer to determine the percent weight of organic matter. The second sample cut from the same horizon of the Woodford core was mechanically polished to obtain a sharp 90° edge using progressively finer standard silicon carbide paper until reaching 4,000 grit then polished with a 1 µm diamond suspension. The sample was subsequently placed inside an SEM and milled with a FIB in order to prepare microcantilever beam geometries. The cantilever beams were then loaded until failure with a Hysitron Pi-85 Picoindenter while imaging via SEM with movies of the tests captured while the load-displacement data was collected.

A Quanta 3D field emission gun (FEG) FIB-SEM was used to prepare the samples. FIB surface milling was used to clean the surface for better sample imaging as well as to prepare the desired microgeometries. Two microcantilevers were manufactured using the following procedures utilized in previously tested materials (Frazer et al. 2015; Maio and Roberts 2005). Each bend bar was shaped by cutting trenches on all three sides with widths of 20 µm and depths of 10 µm using a 15 nA beam current, resulting in a U-shaped trench. The geometry was then refined by applying a 1 nA beam current.

Afterwards, the sample was tilted to 45° along the length axis to shape the cantilever. The base of the cantilever was undercut from both sides using a 3 nA beam current. The resulting cantilever geometry is shown schematically in Figure 3 (a), with the corresponding SEM images of the two microcantilever beams shown in Figure 3 (b) and (c). EDS was performed on the front surfaces of the beams using an Oxford EDS attached to the FIB-SEM.

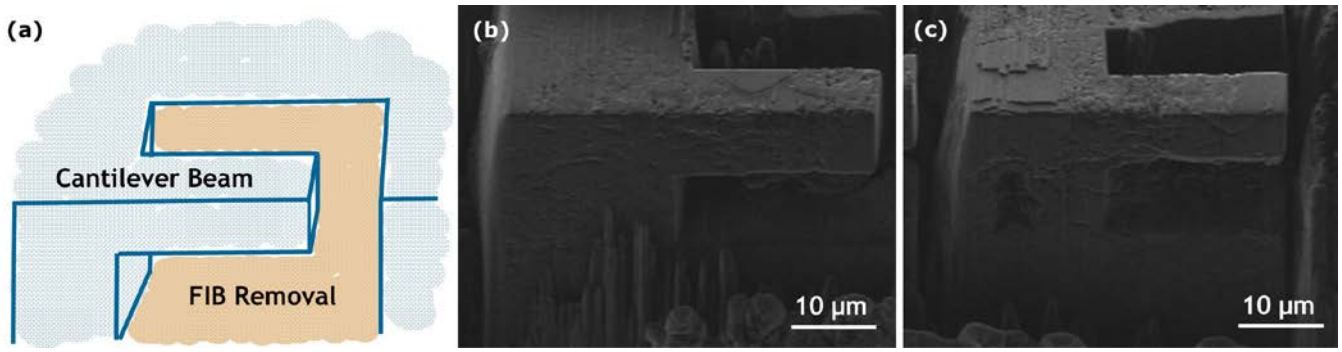


**Figure 3.** The micro-cantilever beam is (a) represented as a schematic showing the regions of shale material which were removed during the milling process with the FIB. SEM images of the micro-cantilever beams are shown for (b) Test B and (c) Test A.

A Hysitron Pi-85 Picoindenter was used to load the microcantilever beams under displacement control mode at 10 nm/s using a 5 µm diamond flat punch indenter tip geometry. All experiments were performed *in situ* under the SEM, and loading of the shale samples continued until failure was observed. For the loading experiment, the indenter tip was placed at the end of the cantilever beam, centered along the y-axis. Figure 4 provides a schematic of the microbeam geometry with dimensions of length L, width b, and height h. When a load of force P is applied to the end of the beam, the cantilever is displaced by distance w.

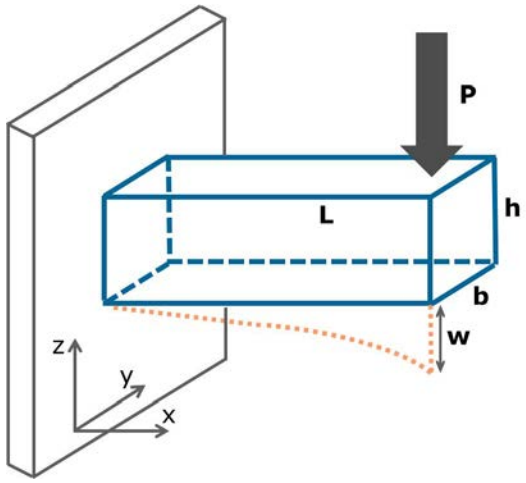


**Figure 4.** The micro-cantilever beam is represented as a schematic showing the labeled dimensions L, b, and h as well as the deformation w and applied force P.

When a solid metallic beam with dimensions in the micron range is subjected to loading, there is a strong evidence of size effects (Chen and Feng 2011). The effects of an intrinsic length $l_{FE}$ on the over all deflection of a solid micro-cantilever beam has been formulated. Although expressions for micro-catilever beams with various loading conditions have been derived, the expression for concentrated load is relevant to our experiments:

$$W = \frac{P x^2 (3L - x)}{6E(I + bhl_{FE}^2)} \quad (1)$$

However, for a granular material with polymer-like strands interspersed throughout the structure, it is not clear what Equation (1) should look like for our KRS micro-cantilever experiments. However, when we assumed $l_{FE}$=0, the above expression turns into the classical theory of beams, and the expression for Young's Modulus, E in, Equation 1 becomes:

$$E = \frac{PL^3}{3wI} \tag{2}$$

where I is the moment of inertia.

## Results

The composition of the Woodford shale sample was determined by a number of methods including XRD, EDS, and TOC analyses. A full suite of Woodford shale characterization is provided in Abousleiman et al. (2007) and can be used as a point of comparison. The mineralogical matrix of the shale horizon of the present study, as determined by XRD, is composed of 64% quartz, 4% feldspar, 2% plagioclase, 1% mica, 12% illite, 12% smectite, 3% carbonate (primarily dolomite), 1% pyrite, and <1% trace minerals such as chlorite and anatase. The material also includes within its matrix approximately 9.9 wt% total organic carbon, which is nearly 20 vol% organic matter.

EDS was performed on the front face of each micro-beam prior to the loading test in order to determine a rough estimate for the local concentrations of each mineral. Figure 5 shows the EDS data collected on the front faces of Test A and Test B. The combined map containing each of the elements analyzed is superimposed on an SEM image of the micro-beam. To the right of the image are individual 2-D maps of the elements, which allows the reader to more easily distinguish between the various minerals included in the structure. Both beams contain calcium/magnesium features far back in the support region corresponding to dolomite, but only micro-beam Test B shows a small amount of dolomite within the beam itself. Also, both beams contain iron sulfide framboids close to the middle of the analyzed area, which fall near the interface between the beam and the support. Finally, when comparing the two beams, it is apparent that there is more carbon in micro-beam A than in B. These features will again appear and be explored after the loading experiment.

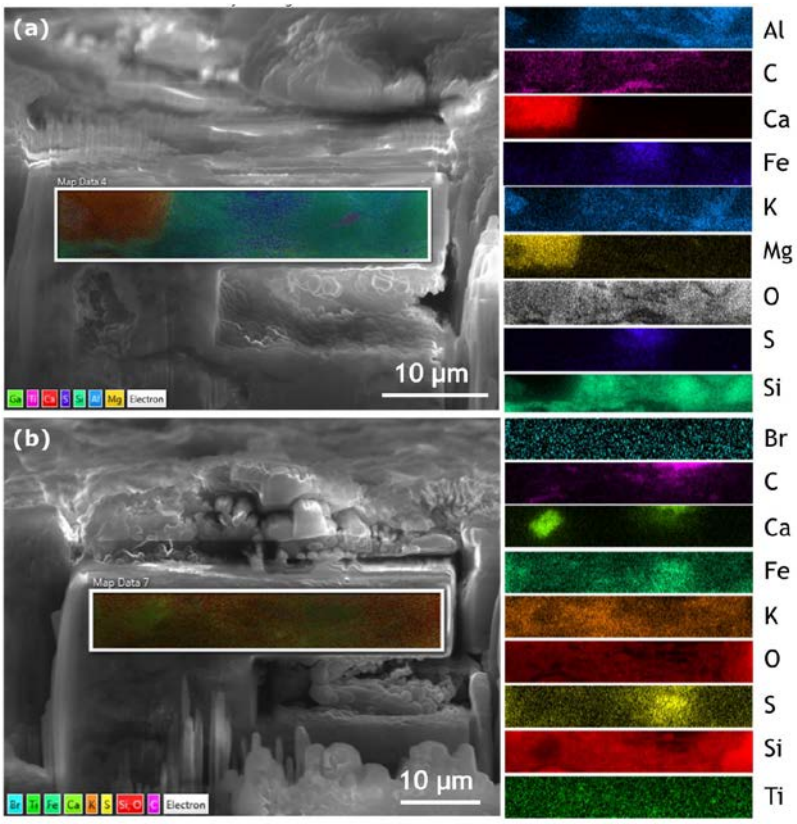


**Figure 5.** EDS data is shown for micro-beam (a) Test A and (b) Test B. Maps with all of the elements are overlaid with the SEM images of each of the micro-beams. The individual elemental maps are also shown to the right.

The first attempt to load and fail kerogen-rich shale beams with micrometer sizes in 3-D dimensions is described here. Given the heterogeneous nature of our composite shale, we were interested to see whether at the microscale (still larger than the REV) each sample would show the same failure mechanism. The two tests were performed inside the SEM with the small-scale nanoindenter, and movies of the loading and failure were captured in real time. This unique experimental setup

provides not only the ability to load and fail micro- and nanoscale shale structures but also the advantage of visualizing the crack initiation, propagation, and ultimate failure of the beams. Subsequent high resolution imaging of the support and beam fracture faces as well as complementary EDS allows us to analyze the minerals and organic matter that are associated with the fracture.

Figure 6 provides a series of load-displacement curves collected during beam Test A with frames (a) through (d) shown in chronological order. Frames (a) and (b) were captured at forces of 700 μN and 2500 μN, respectively, which are in the linear elastic region of the loading curve. As the loading continues, a dip is observed at 3800 μN while a small crack appears on the beam. Then the micro-beam recovered shortly to a load value close to 4050 μN before the noticeable failure shown in frame (c) where the load decreased to almost 3000 μN, as highlighted by the red square. As the loading continues beyond this point, clear strain hardening behavior is observed, while a major fracture develops. However, the micro-beam continues to gain energy before total failure is observed in frame (d). The maximum force achieved corresponds to the ultimate tensile stress, UTS, while the area under the force-displacement curve corresponds to the amount of energy required to fail this micro-beam.

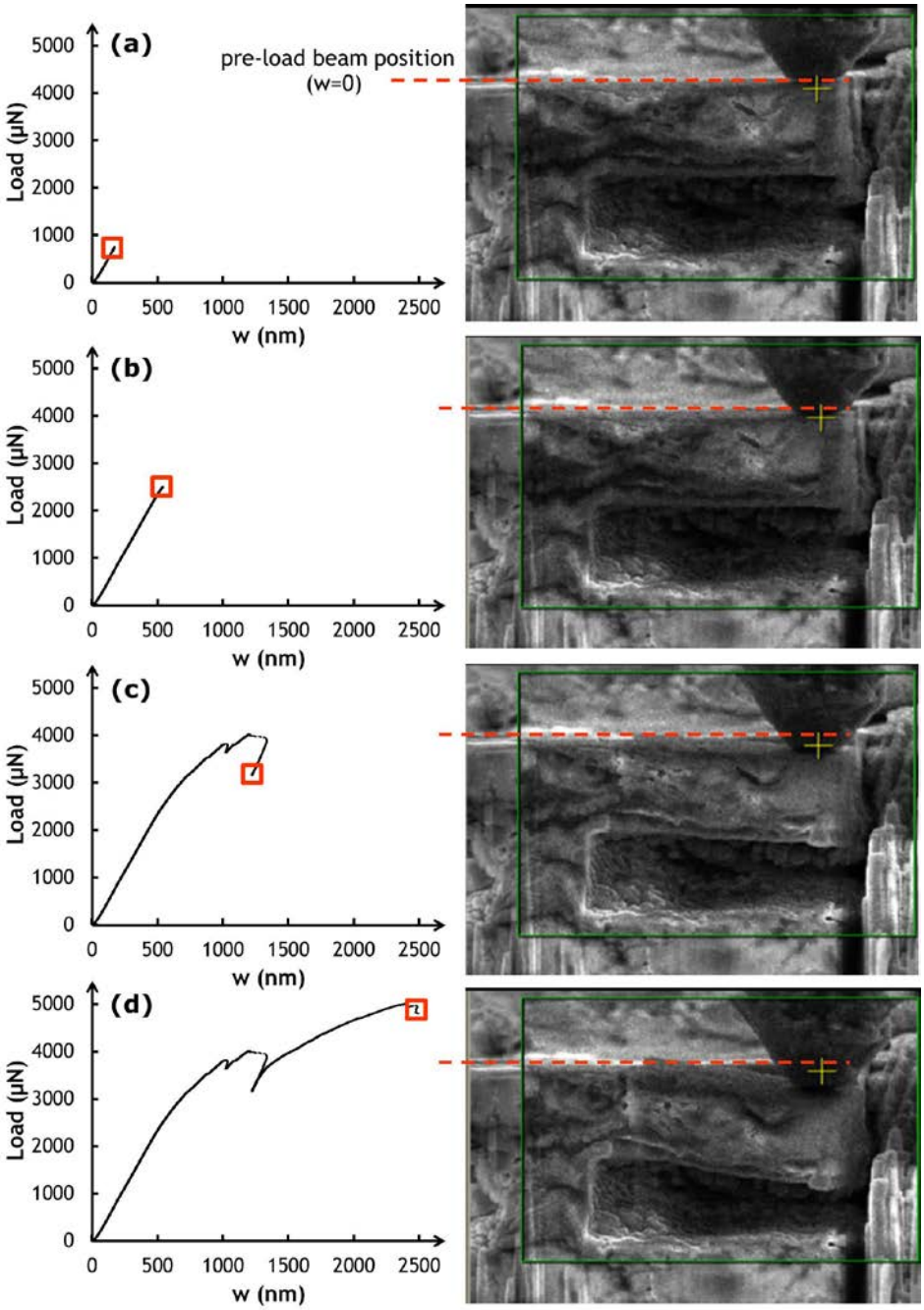


**Figure 6.** The plots of load versus displacement for the microcantilever testing are shown for Test A with frames (a) through

(d) given in chronological order.

The chemical composition of the micro-beam in Test A was also examined using SEM and EDS. A number of observations can be made from the SEM images of Test A shown in Figure 7 (a)-(d). First, panel (a) shows the beam pre-failure from the top view. Panels (b), (c) and (d) show the broken sample from different orientations. In (b), both the beam and the support are shown, whereas (c) and (d) show the support and the beam, respectively, at a much high magnification. The red rectangles in Panels (a), (b), and (d) highlight an inclusion through which the fracture propagated. The identity of this inclusion was determined by EDS as shown in Panel (e). The SEM image in (e) is looking directly at the fracture face of the broken beam and has been rotated such that the inclusion is in the upper right hand corner, and the image is furthermore overlaid with EDS data. To the right, the EDS maps for various elements analyzed are shown and clearly demonstrate that the inclusion is iron sulfide.

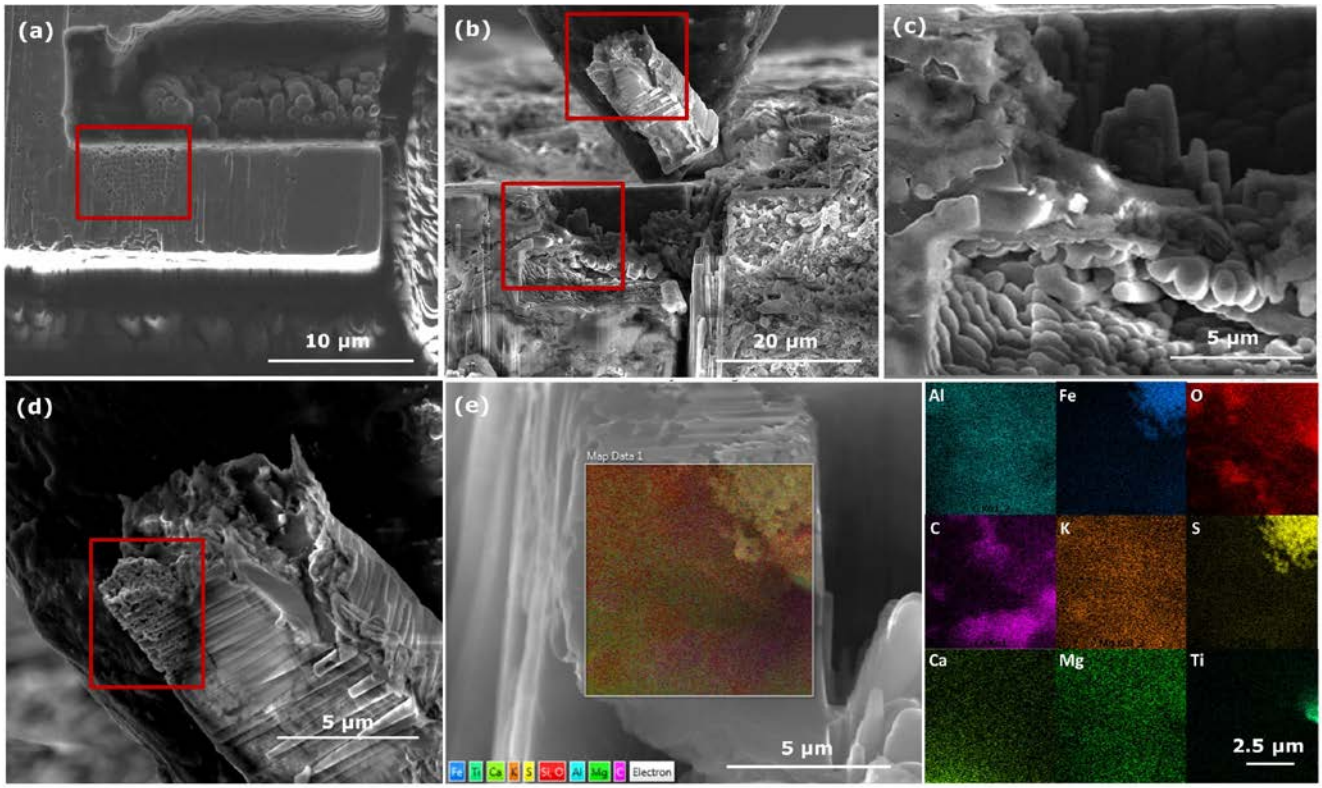


**Figure 7.** Cantilever beam Test A shown from the (a) top view before fracturing. After the micro-beam was fractured, SEM images were captured of (b) the support and beam together as well as (c) the support and (c) the beam individually at higher magnification. The face of the broken support was subsequently analyzed via EDS, as shown in (e).

A second important observation from Test A is the manner in which the micro-beam crack forms and propagates through the structure. First, as the fracture initiates as seen in Figure 6(c), the crack moves transversally from the top of the cantilever near the support towards the bottom of the cantilever. However, as the load continues to increase, the crack eventually takes a turn and moves along the length of the cantilever, propagating horizontally. After the beam has completely failed, the failure pathway becomes quite transparent. In Figure 7(c), there is a large piece of shale sticking out from the bottom of the support region, and a large piece is missing in the broken micro-beam as seen in 7(d). The broken piece of the support was further analyzed by EDS from the front side as shown in Figure 8. From the individual element maps, it can be seen that there is a prominent vane of carbon (kerogen) running through the broken piece of shale all the way out to the tip of the broken structure. Similarly, the presence of a large amount of organic matter in the failure region is supported by the EDS of the failure face in Figure 7(e), where a large amount of carbon is present. As will be described in the proceeding section, the organic matter that was near the support region for this particular cantilever test plays a significant role in influencing the tensile strength characteristics of composite shales such as the Woodford.

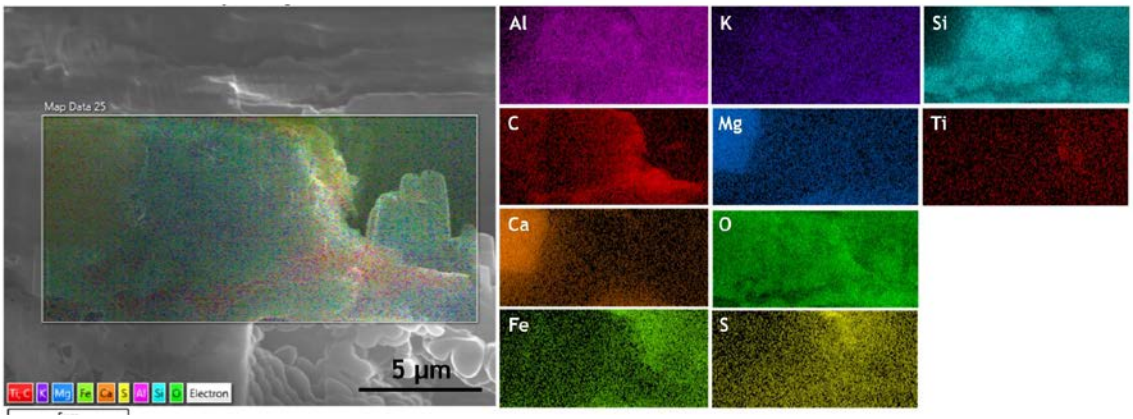


**Figure 8.** EDS data are shown for the broken support of cantilever beam Test A.

Similarly, four frames captured while Test B was in the loading configuration are shown in Figure 9. Whereas Test A required 5000 µN of force to fail the cantilever beam, Test B only required 2200 µN of applied force. Frames (a) through (c) were all collected during linear elastic loading. After reaching an applied load of 2000 µN (corresponding to 650 nm of deflection), the cantilever beam undergoes a small amount of plastic deformation before ultimate failure at w=900 nm. During the entire course of the experiment, it is very difficult to visually detect the changes in this micro-beam because the total deflection pre-failure is very small—on the order of hundreds of nanometers. It is interesting to note that the failure mode exhibited is largely brittle, whereas Test A was more ductile. The huge differences observed will be interpreted in the discussion section.

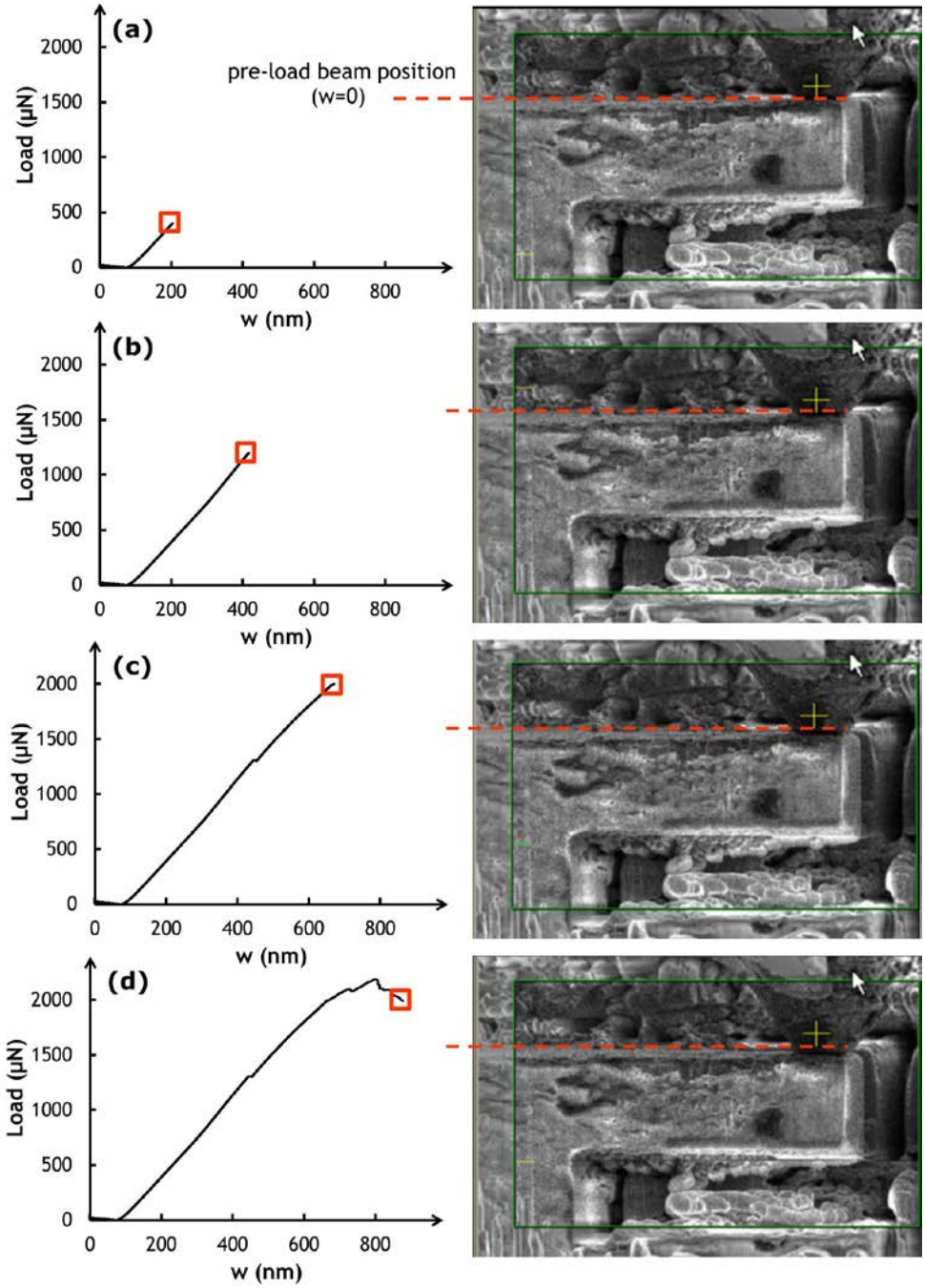


**Figure 9.** The plots of load versus displacement for the microcantilever testing are shown for Test B. Because the beam failed after a small deflection (around 900 nm), it is difficult to detect by eye the nanoscale movement of the beam progressing from frame (a) to frame (d).

Likewise, SEM images of micro-cantilever beam Test B are shown in Figure 10 (a)-(d). Panel (a) shows the Test B beam at pre-loading stage. The indenter is poised above the test specimen but is not yet in contact with the sample. The SEM shown in panel (b) was collected immediately after fracturing the micro-beam, as a transversal crack can be seen near the support region to the left. The same micro-beam is also shown at the post-failure stage in panel (c) from a different angle via the FIB. As the load was released and the indenter was drawn back from the sample, the broken beam attached to the tip as in Test A. Again, as in Test A, an iron sulfide inclusion can be seen on the failure face of the broken beam as shown in Panel (d). The fracture face of the support for Test B was also analyzed by EDS as shown in panel (e), and the iron sulfide cluster is not observed there. This indicates that the fracture propagated entirely around the inclusion and not through it. The EDS of the broken support face furthermore shows the presence of only a small amount of carbon, indicative of a small quantity of organic matter.

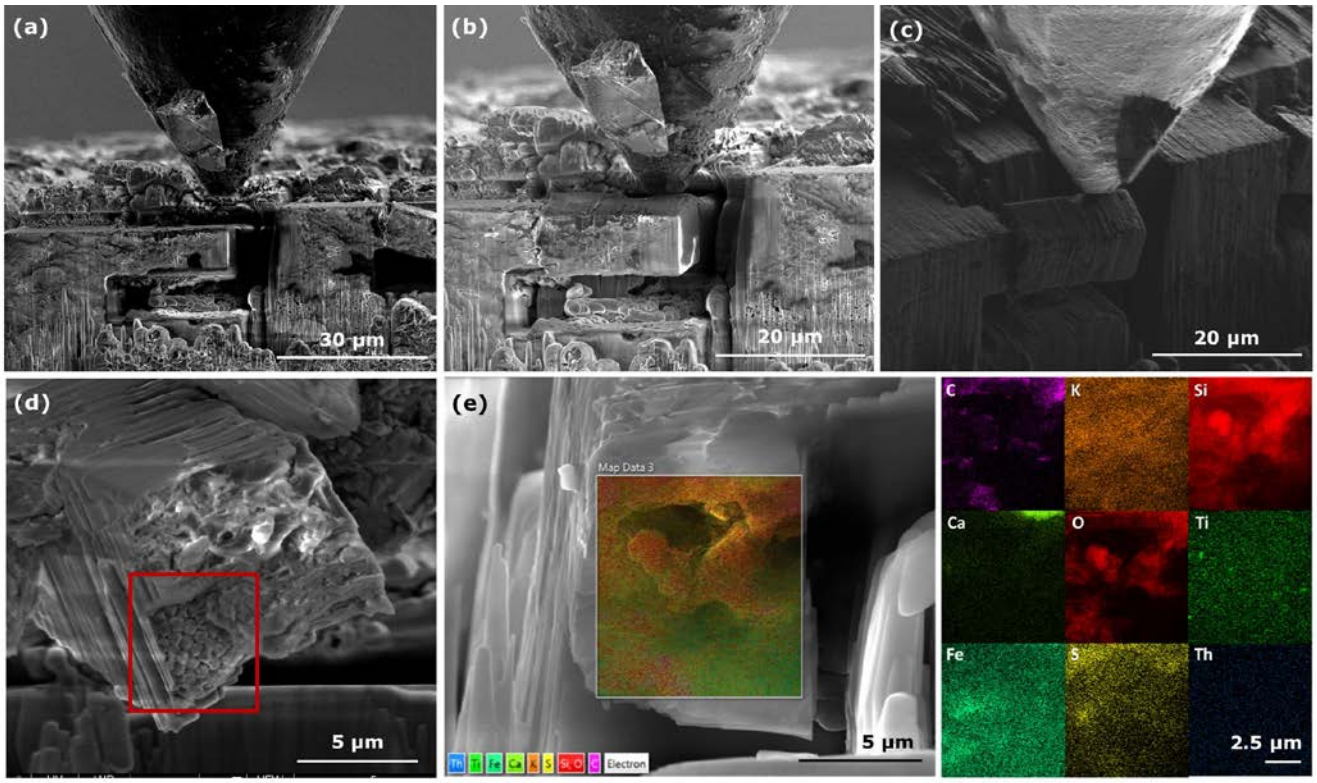


**Figure 10.** SEM images of cantilever beam test B shown from the front view (a) before fracturing and (b,c) after fracturing. The fracture face of the broken beam is shown in (d) while the fracture face of the support was analyzed via EDS as shown in (e).

## Discussion

Tests A and B are not only from the same horizon of the Woodford shale formation, but were also milled within 100 microns of each other. Their different mechanical responses to loading require a deeper understanding of how the heterogeneous shale matrix is influencing the mechanical characteristics. Before complete failure, Beam Test A exhibited significant ductile behavior while Test B underwent only a small degree of plastic deformation. Furthermore, the amount of force and the resulting displacement required to fail each micro-beam were different by more than a factor of two. Determining the reason for these differences is important for us to be able to upscale and convert this information into predictive tools for hydraulic fracturing field applications.

The dimensions of each of the micro-beams that were tested are summarized in Table 1. The beams are similar in size and the corresponding moments of inertia (I) were calculated. For each beam, the applied force P was captured at the halfway point in the linear elastic region. These values were used to calculate Young's Modulus (E, in GPa). Test B has an E that is ~14 GPa, whereas Test A resulted in a much higher value of E at ~30 GPa. The former value is within 10% of the Young's Moduli determined in other studies of Woodford shale (Abousleiman et al. 2007; Bennett et al. 2015). The ultimate tensile load is proportional to the ultimate tensile stress, UTS, which is a value that carries much significance in fracturing source shales. In fact, the UTS is much more important than the unconfined compressive strength (UCS) since hydraulic fracturing is Mode I tensile crack failure rather than a compressive or shear failure.

**Table 1.** The dimensions of each of the cantilever beams are given along with their respective moments of inertia. The forces were obtained from the linear loading curve at the halfway point.

| Symbol | Unit | Description | Test A | Test B |
|---|---|---|---|---|
| L | μm | Beam Length | 21.37 | 23.18 |
| b | μm | Beam Width | 7.36 | 7.95 |
| h | μm | Beam Height | 9.23 | 9.94 |
| I | $\mu m^4$ | Moment of Inertia | 483 | 651 |
| P | μN | Force (Elastic Regime) | 1016 | 478 |
| E | GPa | Young's Modulus | 30.4 | 13.5 |

The differences observed when failing the two beams are best captured by viewing them plotted together. Figure 11 shows Test A and B together with the areas under the load-displacement curves highlighted. The orange area signifies the energy required to fail beam B and the gray area shows the amount of energy needed to rupture beam A. These plots plainly demonstrate that approximately 10 times more energy is needed to fail beam A than beam B. In hydraulic fracturing language, this means that 10 times more energy is needed to pump the fluid into the formation. The ability to identify and capture the true tensile strength of unconventional source rocks on the nano- and micro-scales will have a profound effect upon our field operations.

The reason for the large difference in tensile strength between two specimens from the same sample is easily described by Figures 1 and 2. The organic matter (kerogen, bitumen, etc.) is interwoven with the mineral matrix in a complex manner that spans across nano-, micro-, and macro-scales. The Woodford shale used in the present study contains almost 10 wt% organic matter which corresponds to roughly 20 vol%. This organic matter has rubber- or polymer-like elastomeric qualities, including low compressive strength but high tensile strength. Because the kerogen is interwoven with the clay and non-clay minerals at nano- and micro-scales, determining the tensile strength of the composite material requires testing on the nano- and micro-scales. Recent nanoindentation experiments in Woodford shale along both bedding plane normal and bedding plane parallel directions demonstrated the role of the organic matter matrix in influencing the ratio of elastic to plastic work (Bennett et al. 2015).

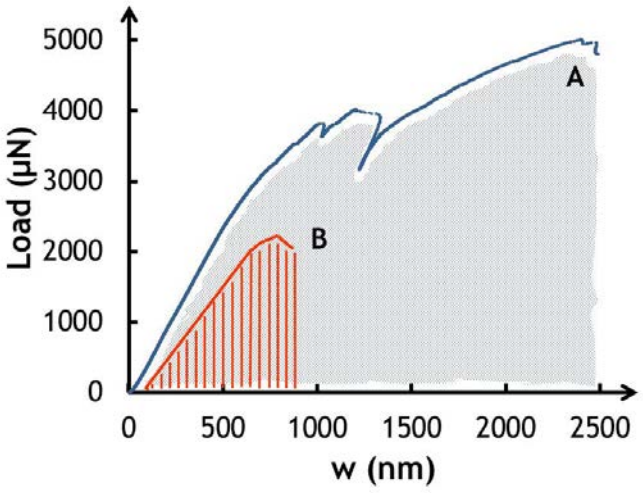


**Figure 11.** Plots of load versus displacement for micro-beam Tests A and B are superimposed on each other. The shading under the curves represents the amount of energy that was required to fail each beam.

In Test B, the micro-beam exhibited largely brittle failure, characteristic of its mineral constituents, and contained very little kerogen in the support/fracture region. In Test A the amount of kerogen was significantly higher and even overwhelming at the support with little volume of the clay or non-clay granular material. The volume of the organic matter that stayed behind at the support is evident by the large cavity left on the micro-beam after total collapse shown in Figure 7 (c) and (d) as well as by the corresponding EDS data shown in Figures 7(e) and 8. The volume of the kerogen was large enough and strong enough to carry the micro-beam into a strain hardening behavior at the post-yield stage, with a huge

modulus of toughness contributing to the overall shale micro-beam behavior. The progress of failure in Test B reinforced our early hypothesis that the cross-linked polymer nature of kerogen and its intertwined structure with the non-clay and clay mineral matrix is the one holding the granular shale matrix together, resulting in large and unexpected values for granular material in tensile failures. Also from Figure 6(c), the fracture has developed almost entirely across the depth of the beam, yet the beam continued taking more load and exhibiting strain hardening until complete failure.

Over the past decade, various macroscale rock mechanics testing methods have been used to characterize source rocks such as shales. However, these methods did not pick up the tensile attributes of these KRS or any other source rock formations. The reason is that the tensile characteristics of polymers are easily masked in the ISRM standard testing methods such as the Brazilian test and other approved tensile strength measurements for rocks. These tests were never designed to isolate or measure the tensile strength of polymer-like materials. This natural cross-linked polymer component, kerogen, with its tensile characteristics, was not known previously to contribute to the tensile strength of any known rock loaded in tension. Now that the organic rich source shale formations are loaded under tensile forces, i.e., Mode I crack opening and crack propagation, the UTS of the organic components is of paramount importance to successfully engineer our lab and field applications.

## Conclusion

For the first time in our industry, the true tensile characteristics of unconventionals have been illuminated. Loading and failing micro-cantilever beams of organic-rich shales provides the correct UTS for the given mineral content, organic matter content and the topology of the constituents. Existing mechanical testing methods cannot account for the properties of the polymer-like kerogen material which is interbedded and interwoven within the mineral matrix. The implications for this discovery are far-reaching. Kerogen, once thought a weak and compliant material, is now understood as strong in tensile loading configurations. In fact, the tensile strength of the organic matter far exceeds that of the surrounding rock matrix. The detrimental effects of this material on the hydraulic fracturing operation also extend beyond raising the requisite energy for fracture initiation to issues involving the long-term productivity of the reservoir such as fracture rehealing. It remains to be seen how this challenge will be addressed in the laboratory in terms of revising our current tensile testing methods as well as in the field where we find methods to lower the overall tensile strength of the composite matrix.

## Acknowledgements

The authors wish to thank Aramco Services Company and Saudi Aramco for permission to publish this research. Our appreciation is also extended to several researchers who have provided valuable services in preparation of this manuscript: Brent Cooper and John Longo (x-ray diffraction), Jordan Kone (SEMs in Figure 1), as well as Daniel Georgi, David Jacobi, and Sebastian Csutak (very helpful discussions). In addition, the authors would like to thank the Biomolecular Nanotechnology Center (BNC) at the University of California, Berkeley (UCB) for use of the FEI Quanta 3D FEG as well as the Geomechanics Gas Shale Consortium (GGSC) for providing the preserved Woodford shale for this work.

## References

Abousleiman, Y., Hull, K., Han, Y., Al-Muntasheri, G., Hosemann, P., Parker, S., Hpward, C.B. 2015.The Granular and Polymer Nature of Kerogen Rich Shale. *Acta Geotechnica* (Submitted).

Abousleiman, Y., Tran, M., Hoang, S., Bobko, C., Ortega, A., Ulm, F.-J. 2007. Geomechanics Field and Laboratory Characterization of Woodford Shale: The Next Gas Play. Presented at the SPE Annual Technical Conference and Exhibition, Anaheim, California, 11-14 November. SPE-110120-MS. http://dx.doi.org/10.2118/110120-MS.

Chalmers GR., Bustin, RM., Power, IM., 2012. Characterization of Gas Shale Pore Systems by Porosimetry, Pycnometry, Surface Area, and Field mission Scanning Electron Microscopy/Transmission Electron Microscopy Image Analyses: Examples from the Barnett, Woodford, Haynesville, Marcellus, and Doig Units. *AAPG Bulletin*, 96(6):1099-119.

Chen S.H., Feng B. 2011. Size Effect in Micro-Scale Cantilever Beam Bending. *Acta Mech*. 219: 291-307. http://dx.doi.org/10.1007/s00707-011-0461-7.

Bennett, K. C., Berla, L.A., Nix, W.D., Borja, R.I. 2015. Instrumented Nanoindentation and 3D Mechanistic Modeling of a Shale at Multiple Scales. *Acta Geotechnica* **10**: 1-14. http://dx.doi.org/10.1007/s11440-014-0363-7.

Curtis, M.E., Ambrose, R.J., Sondergeld, C.H., Rai, C.S. 2010. Structural Characterization of Gas Shales on the Micro- and Nano-Scales. Presented at the Canadian Unconventional Resources & International Petroleum Conference, Calgary, Alberta, 19-21 October. CUSG-SPE-137693-MS. DOI: 10.2118/137693-MS.

Feng, Y., Van Le Doan, T., Pomerantz, A.E. 2013. The Chemical Composition of Bitumen in Pyrolyzed Green River Oil Shale: Characterization by $^{13}C$ NMR Spectroscopy. *Energy & Fuels* 27: 7314-7323. DOI: 10.1021/ef4016685.

Frazer, D., Abad, M.D., Krumwiede, .D, Back, C.A., Khalifa, H.E., Deck, C.P., Hosemann, P. (2015) Localized mechanical property assessment of SiC/SiC composite materials. *Composites: Part A* **70**: 93-101. http://dx.doi.org/10.1016/j.compositesa.2014.11.008.

Hosemann, P., Swadener, J.G., Kiener, D., Was, G.S., Maloy, S.A., Li, N. 2008. An Exploratory Study to Determine Applicability of Nano-Hardness and Micro-Compression Measurements for Yield Stress Estimation. *Journal of Nuclear Materials* 375: 135-143. http://dx.doi.org/10.1016/j.jnucmat.2007.11.004.

Hosemann, P., Martos, J.N., Frazer, D., Vasudevamurthy, G., Byun, T.S., Hunn, J.D., Jolly, B.C., Terrani, K., and Okuniewski, M. 2013. Mechanical Characteristics of SiC Coating Layer in TRISO Fuel Particles. *Journal of Nuclear Materials* 442:133-142. http://dx.doi.org/10.1016/j.jnucmat.2013.08.041.

Ma, J., Couples, G., Jiang, Z., Van Djike, M.I.J. 2014. A Multi-Scale Framework for Digital Core Analysis of Gas Shale at Millimeter Scales, URTeC 1934450. http://dx.doi.org/10.15530/urtec-2014-1934450.

Maio, D.D., and Roberts, S.G. 2005. Measuring Fracture Toughness of Coatings using Focused-Ion-Beam-Machined Microbeams. *J. Mater. Res.* 20: 299-302. http://dx.doi.org/10.1557/JMR.2005.0048.

Oliver, W.C., Pharr, G.M., 1992. An Improved Technique for Determining Hardness and Elastic Modulus using Load and Displacement Sensing Indentation Experiments. *J. Mater. Res.* 19: 3-20. http://dx.doi.org/10.1557/JMR.1992.1564.

Passey, Q.R., Bohacs, K.M., Esch, W.L., Klimentidis, R., Sinha, S. 2010. From Oil-Prone Source Rock to Gas-Producing Shale Reservoir – Geologic and Petrophysical Characterization of Unconventional Shale-Gas Reservoirs. Presented at the CPS/SPE International Oil & Gas Conference and Exhibition, Beijing, China, 8-10 June. SPE-131350-MS. http://dx.doi.org/10.2118/131350-MS.

Schuler, B., Meyer, G., Peña, D., Mullins, O.C., Gross, L. 2015. Unraveling the Molecular Structures of Asphaltenes by Atomic Force Microscopy. *J. Am. Chem. Soc.* 137: 9870-9876. http://dx.doi.org/10.1021/jacs.5b04056.

Ulm, J-F., Abousleiman, Y. 2006. The Nanogranular Nature of Shale. Acta Geotechnica. 1(2):77-88. http://dx.doi.org/10.1007/s11440-006-0009-5.

Zeszotarski, J.C., Chromik, R.R., Vinci, R.P., Messmer, M.C., Michels, R., Larsen, J.W. 2004. Imaging and Mechanical Property Measurements of Kerogen via Nanoindentation. *Geochimica et Cosmochimica Acta* **68**(20): 4113-4119. http://dx.doi.org/10.1016/j.gca.2003.11.031.